Journal of Constructional Steel Research 123 (2016) 53–67

Contents lists available at ScienceDirect

Journal of Constructional Steel Research

Seismic retrofit of special truss moment frames using viscous dampers

Jinkoo Kim *, Joonho Lee [1], Hyungoo Kang [2]

Department of Civil and Architectural Engineering, Sungkyunkwan University, Suwon 440-746, Republic of Korea

ARTICLE INFO

Article history:
Received 22 October 2015
Received in revised form 27 March 2016
Accepted 23 April 2016
Available online xxxx

Keywords:
Special truss moment frames
Seismic performance
Fragility analysis
Viscous dampers

ABSTRACT

The special truss moment frame (STMF) is known to provide higher lateral stiffness with relatively less weight as compared to conventional moment resisting frames. In this study the seismic performance of STMF was investigated by fragility analyses and the results were compared with the performance of special moment resisting frames. Then seismic retrofit scheme was proposed by installing a viscous damper in the special segment to meet enhanced seismic performance objective. The required amount of additional viscous damping was determined based on the nonlinear static procedure provided in the ASCE/SEI 41-10. The analysis results showed that the STMF showed larger stiffness and strength but smaller ductility compared with the moment frames, which resulted in similar seismic fragility in both structures. The seismic performance of STMF with viscous dampers in the special segments turned out to meet the desired target performance, and the effect of adding viscous dampers in the seismic fragility was most significant in the complete damage state.

1. Introduction

The special truss moment frame (STMF) is a seismic load-resisting system that consists of horizontal truss floor beams with specially designed segments that are expected to act as seismic fuses. This framing system is known to provide higher lateral stiffness with relatively less weight as compared to conventional moment resisting frames. Basha and Goel [5] proposed seismic design criteria for the system and carried out experimental study of the STMF system with vierendeel middle segment. They found that the system results in increased economy and inelastic deformation capacity compared with other conventional framing systems. Chao and Goel [6] provided a performance-based plastic design procedure in which the seismic energy demand is balanced with the hysteretic energy dissipation in the special segments. Jordan et al. [13] analyzed STMF systems subjected to seismic load, and proposed modified design procedure for special segments introducing pin connections to the chord members. They found that, compared with conventional STMF systems, significant reduction in axial, shear, and bending moments could be achieved by introducing pin connections. Chao and Goel [6] employed the plastic design method to design chord members in the special segment. They also presented a direct performance-based plastic design method based on an energy concept and plastic design method which requires no iterative evaluation. The procedure begins by selecting a desired yield mechanism for the structure, and the design base shear and lateral forces are determined from spectral energy for a given hazard level. Then the frame members are designed by following the plastic design method. Pekcan et al. [18] proposed a special truss moment frame (STMF) with a buckling restrained brace in a special segment combined with introduction of pin connections at the ends of chord members. The proposed system was

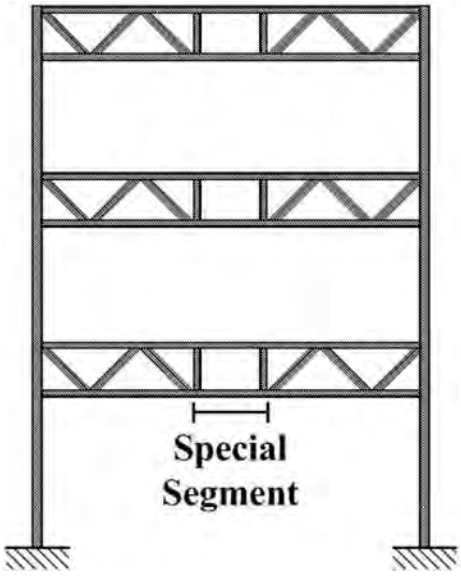

Fig. 1. Typical configuration of a STMF.

* Corresponding author.
E-mail addresses: jkim12@skku.edu (J. Kim), jjoonnoo@nate.com (J. Lee), exult84@gmail.com (H. Kang).
[1] Post-doctoral researcher.
[2] Graduate student.

http://dx.doi.org/10.1016/j.jcsr.2016.04.027
0143-974X/

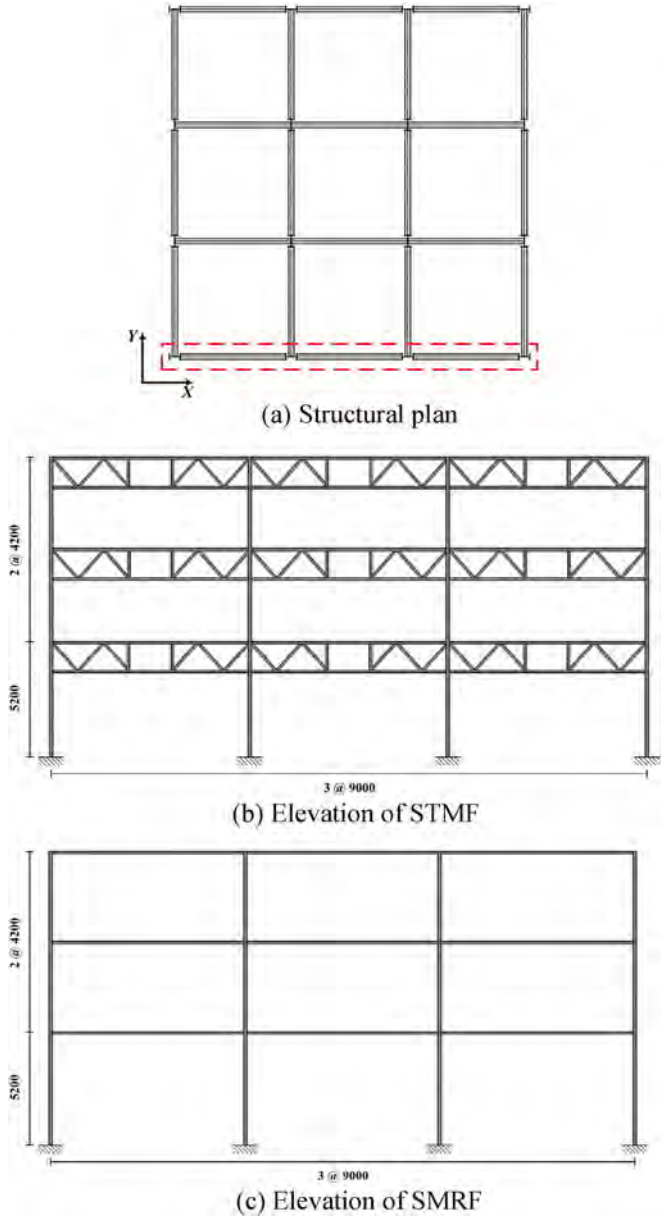

Fig. 2. Configuration of analysis model structures.

found to show more predictable seismic response and cost savings due to reduced member forces. Ölmez and Topkaya [17] carried out finite element analysis of STMF and found that the expected shear strength formulation presented in the AISC Seismic Provisions for Structural Steel Buildings was overly conservative. Based on the analysis results they proposed a new expected shear strength formula for STMF. Pekcan et al. [19] proposed a design procedure of special truss moment frame (STMF) with a buckling restrained brace in a special segment based on the performance-based plastic design procedure. In their study the chord members in the special segments were assumed to be pin connected and the diagonal BRBs were designed to dissipate all seismic input energy. Kim and Park [15] investigated the progressive collapse potential of the special truss moment frames and proposed a design procedure to provide an alternate load path in the case of sudden column removal. It was shown that the model structures redesigned using the developed design procedure turned out to remain stable after a column was suddenly removed. Recently, Heidari and Gharehbaghi [12] proposed a new configuration of STMF systems including buckling resistant braces located at the side of beam-column connections as the top and bottom members of truss-girders. They showed that the proposed configuration of STMF with buckling resistant braces improved the seismic safety of STMF. Currently, STMF is considered as one the seismic force-resisting systems in the ASCE 7-13 [3], and the design process is provided in the ANSI/AISC 341-10 specification [1].

Viscous dampers have been widely used to mitigate earthquake induced damage of structures effectively. Lavan and Levy [16] carried out performance based optimal seismic retrofitting of yielding plane frames using added viscous damping devices. They derived the gradients of the constraints with respect to the damping coefficients via optimal control theory, and obtained the optimal solution by assigning damping only to stories for which the local performance index has reached the allowable value. Silvestri et al. [24] investigated seismic design procedure of a precast RC structure equipped with viscous dampers. They confirmed the effectiveness of viscous dampers as compared with traditional lateral-resisting stiff braces for the seismic design of precast concrete structures. Kim et al. [14] investigated the feasibility of using viscous dampers for preventing progressive collapse of building structures. They found that the viscous dampers, designed to reduce earthquake-induced vibration, were effective in reducing vertical displacement of the structures caused by sudden removal of a column. Serror et al. [23] proposed the seismic force reduction factor for steel moment resisting frames with supplemental viscous dampers. A parametric study was performed using time history analyses and the N2-method, and an equation was proposed for reduction factors based on regression analysis. Recently, Farghaly et al. [11] investigated the seismic performance of two adjacent buildings with different heights connected with viscous dampers. They found that the response of connected structures system founded on soft soil is more critical than those founded on stiff soil. Tzimas et al. [26] carried out seismic design and assessment of steel self-centering moment-resisting frames (SC-MRFs) with viscous dampers within the framework of Eurocode 8 (EC8) and showed that the SC-MRFs with viscous dampers have superior collapse

Table 1
Member sizes of STMF model structures.

		Conner columns	Exterior columns	Exterior chords	Exterior diagonal member	Exterior vertical member
3-story	1F	W10 × 68	W14 × 176	2 L5 × 5 × 5/8 × 3/8	2L3 × 3 × 5/16 × 3/8	2L8 × 8 × 5/8 × 3/8
	2F	W8 × 67	W12 × 120	2 L5 × 5 × 1/2 × 3/8	2L3 × 3 × 1/4 × 3/8	2L6 × 6 × 5/8 × 3/8
	3F	W8 × 31	W10 × 100	2 L4 × 4 × 1/2 × 3/8	2L2 − 1/2 × 2 − 1/2 × 1/4 × 3/8	2L5 × 5 × 3/8 × 3/8
10-story	1F	W14 × 257	W14 × 730	2L6 × 6 × 7/8 × 3/8	2 L3 − 1/2 × 3 − 1/2 × 3/8 × 3/8	2L8 × 8 × 1 − 1/8 × 3/8
	2F	W14 × 176	W14 × 370	2L6 × 6 × 3/4	2 L3 − 1/2 × 3 − 1/2 × 3/8 × 3/8	2L8 × 8 × 1 × 3/8
	3F	W14 × 159	W14 × 342	2L6 × 6 × 7/8 × 3/8	2 L3 − 1/2 × 3 − 1/2 × 3/8 × 3/8	2L8 × 8 × 1 × 3/8
	4F	W14 × 132	W14 × 311	2L6 × 6 × 3/4 × 3/8	2 L3 − 1/2 × 3 − 1/2 × 3/8 × 3/8	2L8 × 8 × 1 × 3/8
	5F	W14 × 109	W14 × 283	2L6 × 6 × 5/8 × 3/8	2 L3 − 1/2 × 3 − 1/2 × 5/16 × 3/8	2L8 × 8 × 7/8 × 3/8
	6F	W14 × 90	W14 × 257	2L6 × 6 × 9/16 × 3/8	2 L3 − 1/2 × 3 − 1/2 × 5/16 × 3/8	2L8 × 8 × 7/8 × 3/8
	7F	W12 × 79	W14 × 233	2L5 × 5 × 5 / 8	2 L3 − 1/2 × 3 − 1/2 × 5/16 × 3/8	2L8 × 8 × 3/4 × 3/8
	8F	W10 × 68	W14 × 193	2L5 × 5 × 1/2 × 3 / 8	2L3 × 3 × 5/16 × 3/8	2L8 × 8 × 7/8 × 3/8
	9F	W8 × 48	W14 × 132	2L4 × 4 × 5/8 × 3 / 8	2L3 × 3 × 1/4 × 3/8	2L6 × 6 × 5/8 × 3/8
	10F	W8 × 48	W10 × 88	2L4 × 4 × 7/16 × 3 / 8	2 L2–1/2 × 2–1/2 × 1/4 × 3/8	2L5 × 5 × 7/16 × 3/8

resistance compared to conventional steel MRFs even when the SC-MRF is significantly lighter than the conventional MRF.

In this study the seismic performance of STMF was investigated by fragility analyses and the results were compared with the performance of special moment resisting frame (SMRF). Then the seismic retrofit scheme of installing a viscous damper in the special segment to meet an enhanced seismic performance level was validated. In this study the required amount of additional viscous damping was determined based on the nonlinear static procedure provided in the ASCE/SEI 41-10 [4]. The plastic hinge formation and the probabilities of reaching various damage states were compared with those of the STMF structures without viscous dampers. The probabilities of reaching various limit states in the STMF structures without and with viscous dampers were computed through fragility analysis and based on the results conclusions were drawn on the effectiveness of viscous dampers for enhancement of seismic performance of STMF structures.

2. Design of model structures

It is specified in the ANSI/AISC [1] that panels within a special segment of STMF should either be all vierendeel panels or all X-braced panels. The section at the ends of the special segment will be subjected to significant flexural yielding and dissipate hysteretic energy during seismic events, and thus they are required to sustain large cyclic strains. Fig. 1 depicts the typical configuration of a STMF with a special segment composed of a vierendeel panel. The Seismic Provisions for Structural Steel Buildings, ANSI/AISC 341-10 [1], requires that STMF is designed to withstand significant inelastic deformation within a special segment of the truss when subjected to the design earthquake load. Members outside the special segment are required to remain elastic, and are designed per the AISC Specification for Structural Steel Buildings [2].

The first step to design a STMF is to determine the vertical shear associated with the special segments subjected to design loads. Members outside the special segment are designed for forces generated by the fully yielded chords of the special segment plus the corresponding gravity loads. Columns are designed to resist the available shear strength of the special segment, thus assuring a strong column-weak beam system [10]. The AISC Seismic Provisions requires that the span length of STMF between columns and the overall depth do not exceed 20 m and 1.8 m, respectively. It is also required that chord members in the special segment should be compact cross sections to facilitate the formation of plastic hinges. They specify that the members of STMF located outside of those in the special segments are designed for the lateral loads necessary to develop the expected vertical shear strength of the special segment V_{ne} obtained as follows:

$$V_{ne} = \frac{3.60R_yM_{nc}}{L_s} + 0.036EI\frac{L}{L_S^3} + R_y(P_{nt} + 0.3P_{nc})\sin\alpha \quad (1)$$

where E = modulus of elasticity of a chord member of the special segment, I = moment of inertia of a chord member of the special segment, L = span length of the truss, L_s = length of the special segment, M_{nc} = nominal flexural strength of a chord member of the special segment, P_{nt} = nominal tensile strength of a diagonal member of the special segment, P_{nc} = nominal compressive strength of a diagonal member of the special segment, R_y = ratio of the expected yield stress to the specified minimum yield stress, and α = angle of diagonal members with the horizontal plane.

Table 2
Member sizes of SMRF model structures.

		Conner columns	Exterior columns	Exterior beams
3-story	1F	W10 × 60	W12 × 87	W21 × 48
	2F	W10 × 60	W12 × 87	W21 × 48
	3F	W10 × 60	W12 × 87	W21 × 48
10-story	1F	W14 × 145	W14 × 233	W21 × 93
	2F	W14 × 120	W14 × 233	W21 × 93
	3F	W14 × 120	W14 × 211	W21 × 93
	4F	W14 × 90	W14 × 211	W21 × 73
	5F	W14 × 90	W14 × 176	W21 × 73
	6F	W12 × 87	W12 × 159	W21 × 68
	7F	W12 × 79	W12 × 159	W18 × 55
	8F	W12 × 72	W12 × 120	W18 × 55
	9F	W12 × 72	W12 × 106	W16 × 50
	10F	W12 × 65	W12 × 106	W16 × 50

Table 3
The period of analysis models (sec.)

	STMF	SMRF
3-story	0.72	1.23
10-story	1.38	2.31

Fig. 2 shows the structural plan and elevation of the analysis model structures composed of three and ten story STMF. The special moment resisting frame (SMRF) designed with the same loading condition

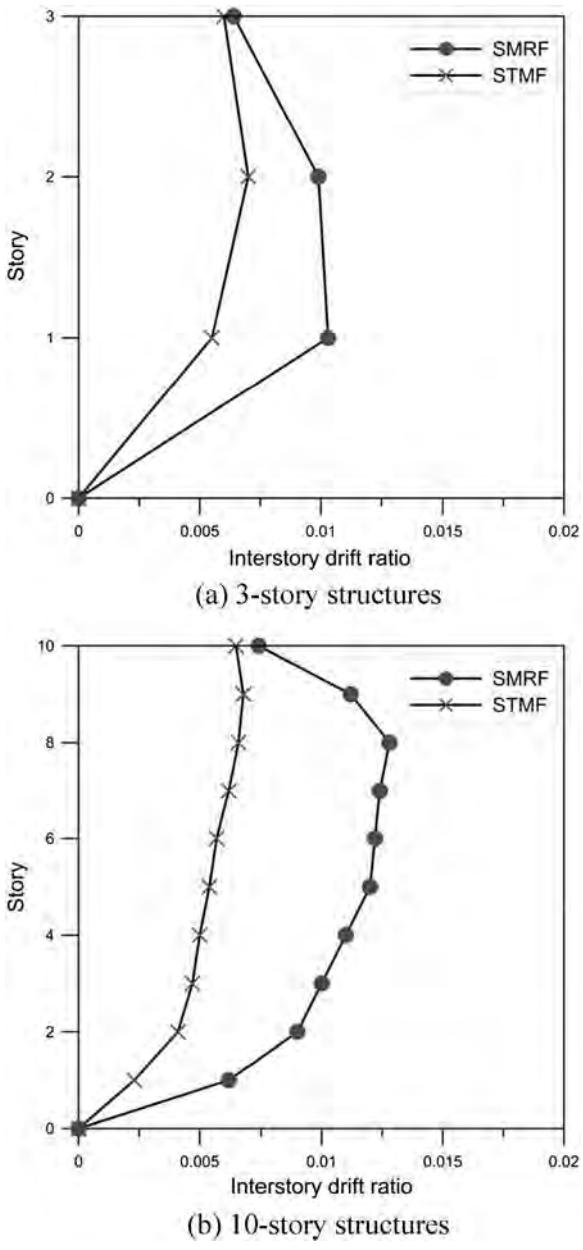

Fig. 3. Inter-story drift ratios of the model structures subjected to design seismic load.

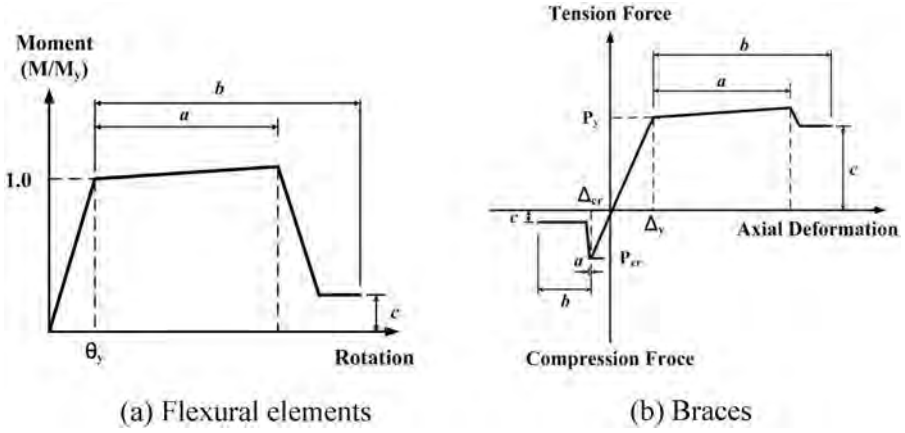

Fig. 4. Nonlinear force-displacement relationships of structural elements.

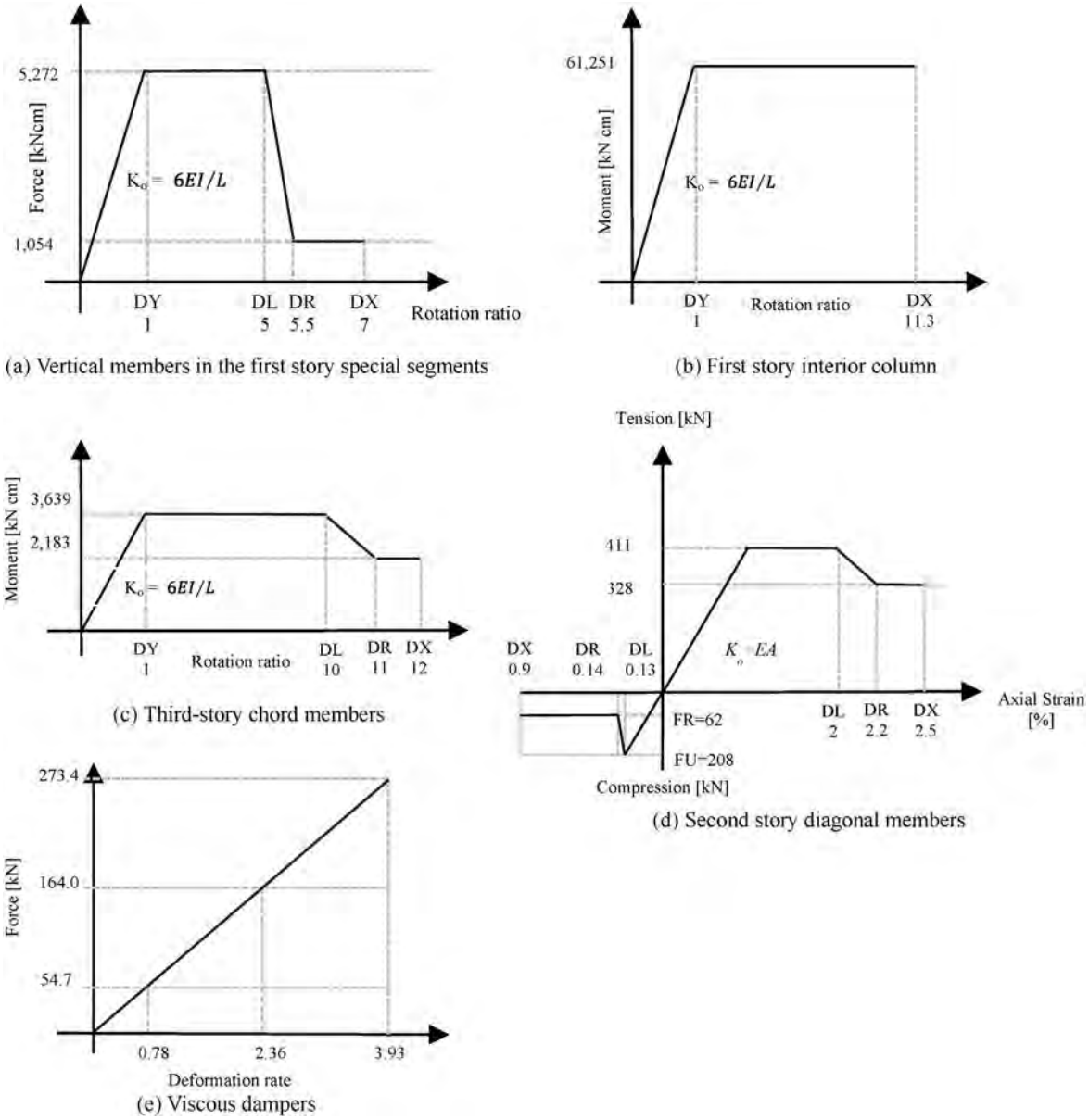

Fig. 5. Nonlinear force-displacement relationships of selected structural elements.

were also analyzed for comparison. Only the exterior frame marked on the structural plan was analyzed for simplicity. The model structures were designed to resist dead and live loads of 4.9 kN/m^{2}and 2.5 kN/m^2, respectively. The design seismic load was obtained following ASCE/SEI 7-13 procedure using the spectral acceleration coefficients S_{DS} and S_{D1} equal to 0.43 and 0.23, respectively. The response modification factors were determined as 7.0 and 8.0 for STMF and SMRF, respectively, as specified in ASCE/SEI 7-13. The chord members of STMF and beams in SMRF were designed using structural steel with yield and ultimate strength of 235 and 400 N/mm^2, and the other members were designed with steel having yield and ultimate strength of 325 and 490 N/mm^2, respectively. The truss elements in STMF were designed with double angle sections, and the columns were made of wide flange sections. All members in the SMRF structures were composed of wide flange sections. The chord members in the special segments of the STMF model structures were designed first using the member forces imposed by the design loads. Then the maximum vertical shear strength, V_{ne}, were computed using Eq. (1). The last term of Eq. (1) was not applied because there was no diagonal member in the special segments. The equivalent lateral loads were computed using the maximum shear forces in the special segments, and the other members were designed using the equivalent lateral loads plus the factored gravity loads.

Table 1 and Table 2 show the sizes of selected structural members of the STMF and SMRF structures, and Table 3 shows the fundamental periods of the model structures. It can be observed that the natural periods of the STMF structures are significantly higher than those of the moment frames. Fig. 3 shows the inter-story drift ratios of the model structures subjected to the design seismic load. The drift ratios were obtained after multiplying the elastic displacement with the corresponding displacement amplification factors. It can be observed that the inter-story drifts of the SMRF are higher than those of the STMF; however even the inter-story drifts of the STMF structures are within the 1.5% of the story height in both the 3- and 10-story structures.

3. Nonlinear analysis results of model structures

Nonlinear static and dynamic analyses were conducted using the program code PERFORM-3D [21]. The force-displacement relationships of structural elements recommended in ASCE/SEI 41-10 [4], which are depicted in Fig. 4, were used in the analysis. The modeling parameters *a*, *b*, and *c*, and the acceptance criteria IO (Immediate Occupancy), LS (Life Safety), and CP (Collapse Prevention) were determined based on the information provided in Tables 5–6 of the provision. The yield rotations of beams and columns were determined using the following Eq. 2(a) and (b), respectively, which are also provided in ASCE/SEI 41-10 [4] Eq. 5a, b:

$$\theta_y = \frac{ZF_{ye}l_b}{6EI_b} \quad \theta_y = \frac{ZF_{ye}l_c}{6EI_c}\left(1-\frac{P}{P_{ye}}\right) \qquad (2(a,\ b))$$

where θ_y = yield rotation, E = modulus of elasticity, F_{ye} = expected yield strength of the material, I = moment of inertia, l_b = beam length, l_c = column length, P = axial force in the member at the target displacement for nonlinear static analyses, and P_{ye} = expected axial yield force of the member which is equal to A_gF_{ye}. The beams (upper and lower chords of the truss) and columns were modeled by the FEMA beam steel type, and the diagonal members were modeled by the inelastic bar elements. The viscous dampers were modeled using the fluid damper elements in the PERFORM 3D. The nonlinear force-displacement relationships for selected members are depicted in Fig. 5. In Fig. 5(a) the horizontal axis represents the ratio of the member rotation with respect to the yield rotation which is computed automatically in the PERFORM 3D from the given yield moment and the stiffness. The abscissa of the force-displacement curve for the other elements is represented similarly.

3.1. Nonlinear static analysis

Nonlinear static pushover analyses of the model structures were carried out using the lateral loads distributed vertically proportional to the fundamental natural periods. Fig. 6 shows the pushover curves of the model structures, where the design base shear and the points of first plastic hinge formation and strength loss in special segments are also indicated. Fig. 7 depicts the plastic hinge formation at the maximum inter-story drift of 4% of story height. The plastic hinge rotations are divided into the IO, LS, and CP limit states as defined in ASCE/SEI 41-10. It can be observed that STMF model structures generally have larger stiffness and strength than those of the SMRF structures. In the 3-story STMF structure plastic hinges first formed at the first and the second story special segments. When the strength reached the maximum point, plastic hinge formed at the third story special segment. The first strength drop occurred when the plastic rotation in the second story special segments exceeded the collapse prevention limit state. The strength dropped again when the rotation of the plastic hinges in the first story special segments reached the limit state. At the maximum inter-story drift of 3% plastic hinge formed at the first and the third

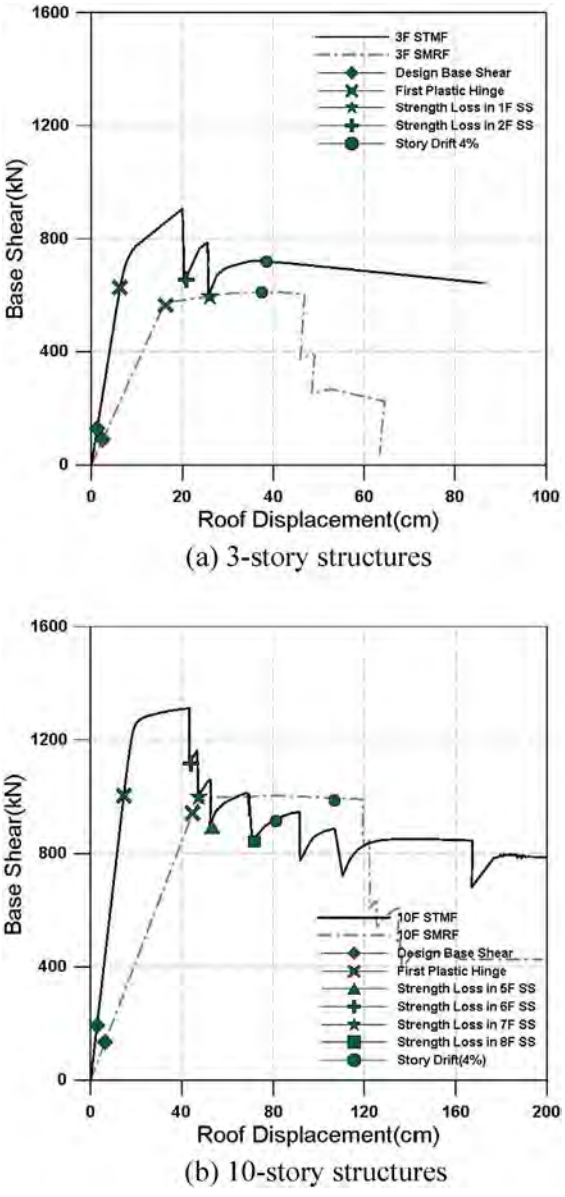

Fig. 6. Pushover curves of analysis model structures.

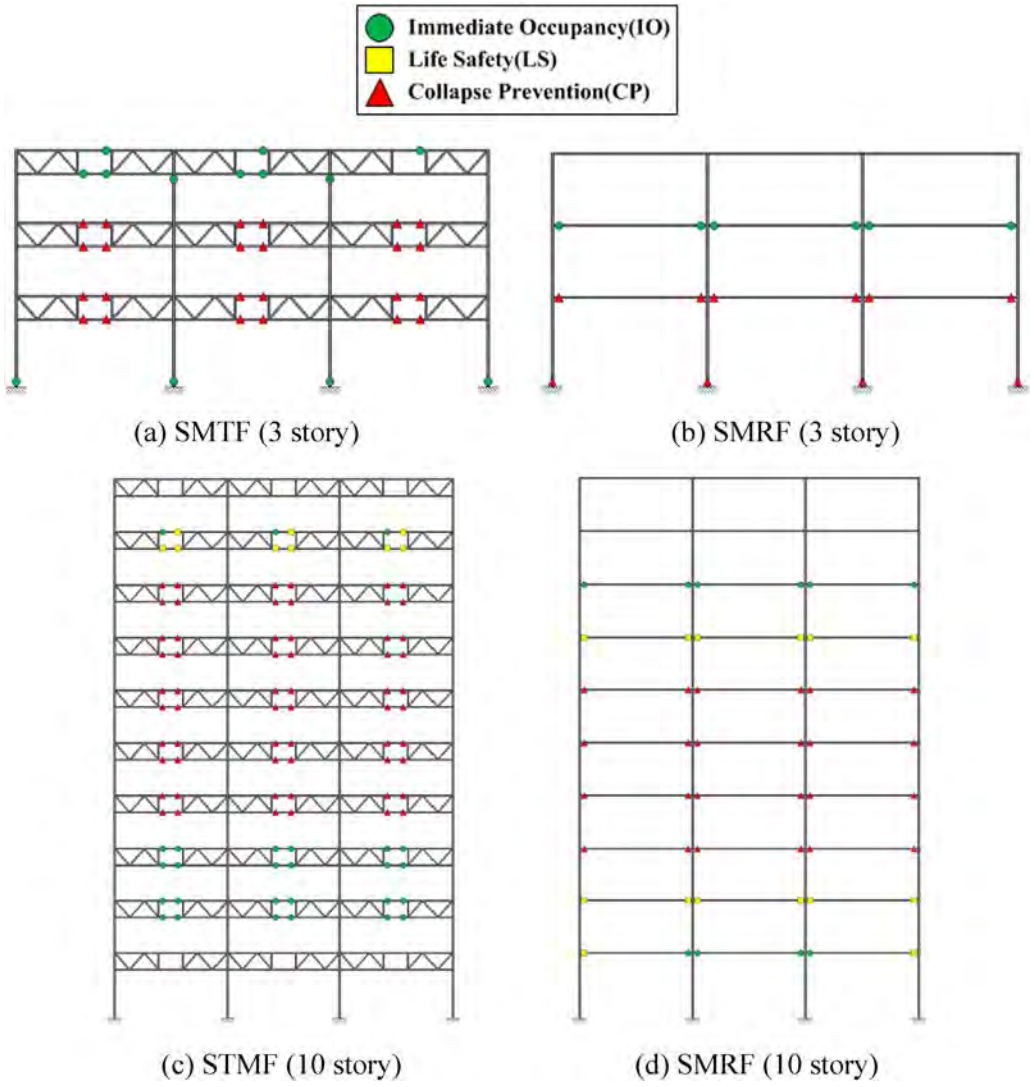

Fig. 7. Plastic hinge formation at the maximum inter-story drift of 4%.

story columns. In the 10-story STMF structure the yield of structural members started at the 7th story special segment. Then plastic hinges formed at special segments located in the 2nd to 9th stories. At the maximum strength the plastic deformation in the 6th story special segment reached the collapse prevention limit state and the strength dropped sharply. Then the limit state was reached at the 7th, 5th, and 8th story special segments which leaded to continuous decrease in strength. In the 3-story SMRF structure plastic hinges first formed in the first story beams and columns and spread to the second story beams. In the 10-story structure plastic hinges first formed in the 5th-story beams and spread to the beams throughout the stories.

The global damage states of the model structures were divided into four levels such as Slight, Moderate, Extensive, and Complete damage.

Table 4
Maximum inter-story drift ratios corresponding to the damage states obtained from pushover analysis.

	3-story STMF	3-story SMRF	10-story STMF	10-story SMRF
Slight	0.0042	0.0103	0.0037	0.0092
Moderate	0.0061	0.0149	0.0054	0.0135
Extensive	0.0094	0.0247	0.0091	0.0231
Complete	0.0221	0.0571	0.0214	0.0522

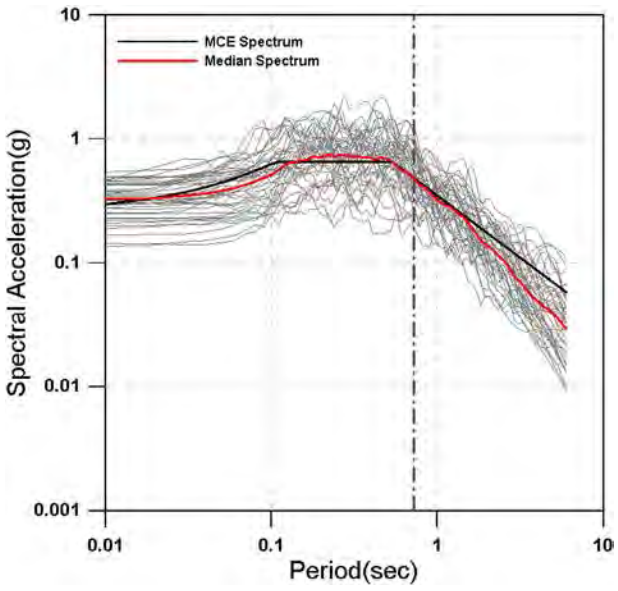

Fig. 8. Response spectra of 44 earthquake records scaled to the natural period of the 3-story STMF structure.

The states of 'Slight Damage' and 'Moderate Damage' were defined as the spectral displacements corresponding to 70% and 100% of yield point, respectively. The 'Extensive Damage' was defined as the quarter point from 'Moderate' to 'Complete' damage. The 'Complete Damage' was the spectral displacement at which the strength decreased to 80% of the maximum strength. Table 4 shows the maximum inter-story drift ratios of the model structures at each damage state.

3.2. Fragility analysis results

A seismic fragility curve typically represents the probability of a system reaching a limit state as a function of a seismic intensity measure. In this study fragility analysis was carried out to compare the probabilities of STMF and SMRF to reach a common limit state. Spectral acceleration was used as a seismic intensity measure, and the seismic fragility was obtained from incremental dynamic analyses carried out using the twenty two pairs of scaled records obtained from the PEER (Pacific Earthquake Engineering Research Center) NGA Database [20]. Damping ratios of 5% were used for all vibration modes. Fig. 8 shows the response spectra of the 44 far field earthquake records, which were used in the incremental dynamic analyses of the 3-story STMF model structure. The median spectrum for the records and the design spectrum for the Maximum Considered Earthquake (MCE) are also depicted in the figure. They were scaled in such a way that the spectral acceleration of each record at the fundamental period of the structure, which is 0.72 s, becomes the same with that of the design spectrum for the Maximum Considered Earthquake (MCE). Fig. 9 and Fig. 10 depict the incremental dynamic analysis results of the STMF and SMRF model structures,

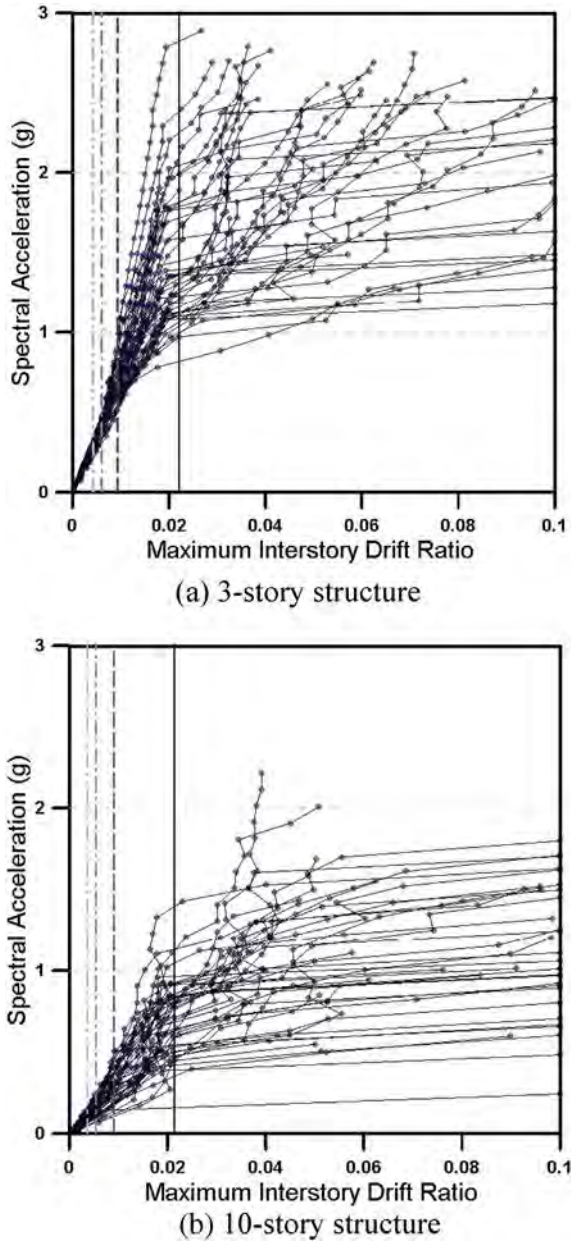

Fig. 9. Incremental dynamic analysis results of STMF structures.

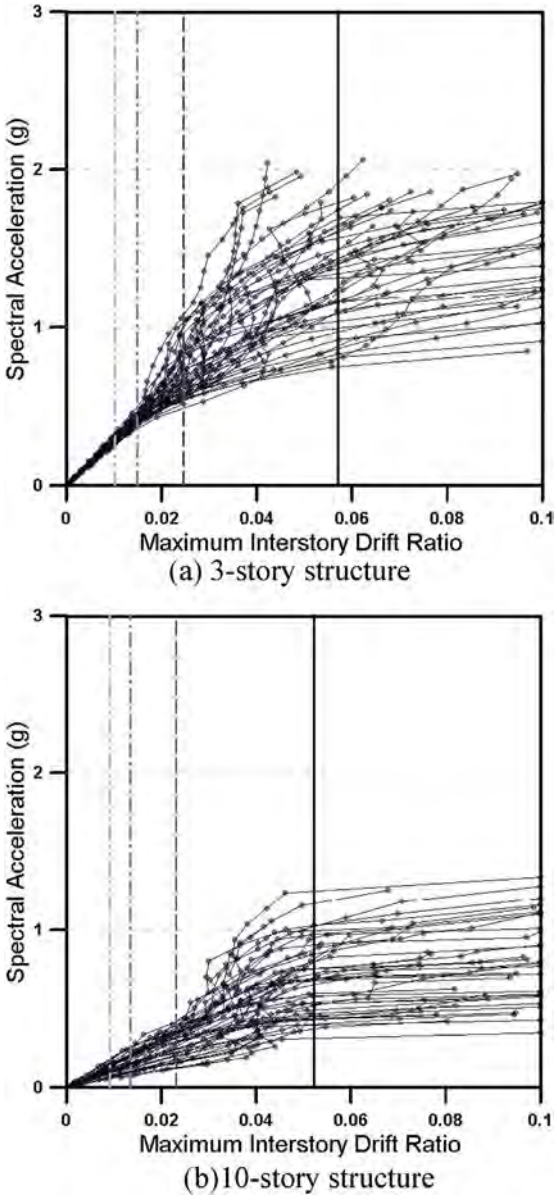

Fig. 10. Incremental dynamic analysis results of SMRF structures.

Table 5
Median structural capacity of the model structures, $\hat{C}$ associated with each damage state obtained from incremental dynamic analyses (g).

	Slight	Moderate	Extensive	Complete
3-story STMF	0.31	0.44	0.66	1.32
3-story SMRF	0.29	0.42	0.63	1.34
10-story STMF	0.10	0.15	0.28	0.71
10-story SMRF	0.10	0.15	0.28	0.69

respectively, in which the spectral accelerations and the corresponding maximum inter-story drift ratios were plotted. The four vertical lines shown in the figures indicate the inter-story drift ratios associated with the limit states. Table 5 shows the median structural capacity $\hat{C}$ associated with the four limit states obtained from the incremental dynamic analysis results of the 44 earthquake records. It can be observed that, even though STMF structures have higher stiffness and strength, the median capacities of the STMF structures associated with the four limit states are quite similar to those of the SMRF structures. This is due to the fact that the ductility capacity of the STMF is smaller than that of the SMRF.

The seismic fragility is described by the conditional probability that the structural capacity, C, fails to resist the structural demand, D, given the seismic intensity hazard, and is modeled by a lognormal cumulative distribution function as follows [8]:

$$P[D \geq C] = \Phi\left(\ln\left[D/\hat{C}\right]/\beta_c \right) \tag{3}$$

where $\Phi[\cdot]$ = standard normal probability integral, $\hat{C}$ = median structural capacity associated with the limit state, and β_C = uncertainty in C for which the total system collapse uncertainty. In this study $\beta_C = 0.6$ was used based on the recommendation of FEMA P695 [9].

Figs. 11 and 12 depict the fragility curves of the STMF and SMRF model structures, respectively, obtained from Eq. (3). It can be observed that the probabilities of reaching a limit state of STMF are similar to those of the SMRF structures. This implies that STMF structures ensure equivalent safety against earthquakes. In both STMF and SMRF structures the fragilities of the 10-story structures turned out to be higher than those of the 3-story structures.

4. Seismic retrofit of STMF with viscous dampers

Various energy dissipation devices have been applied in structures to mitigate wind or earthquake induced vibration [22]. In most cases they are installed between columns and are activated by occurrence of

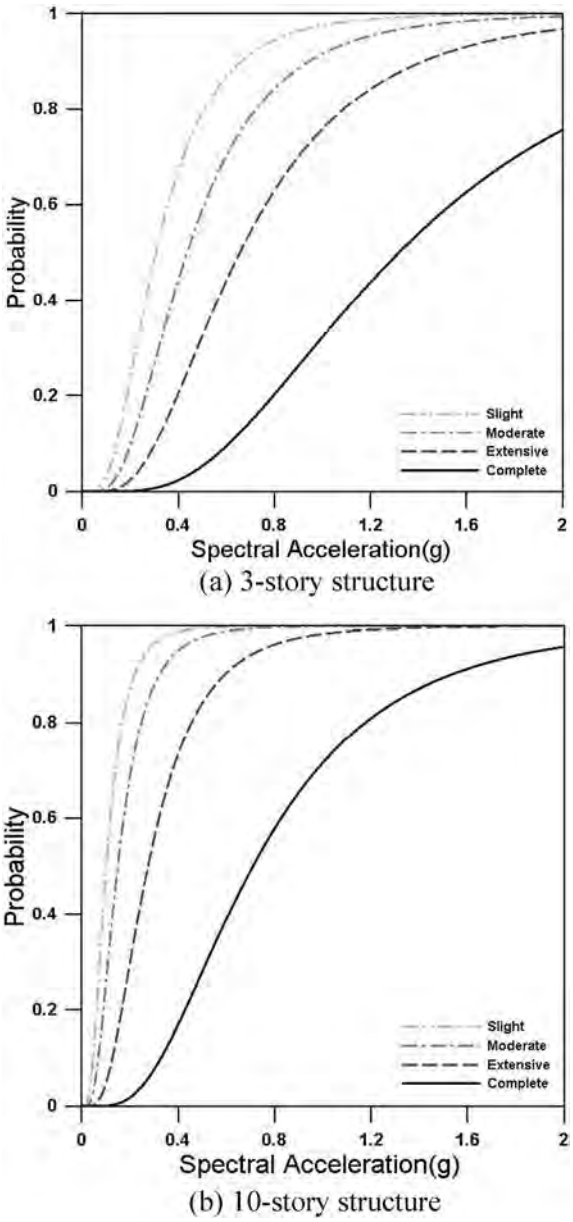

Fig. 11. Fragility curves of STMF model structures.

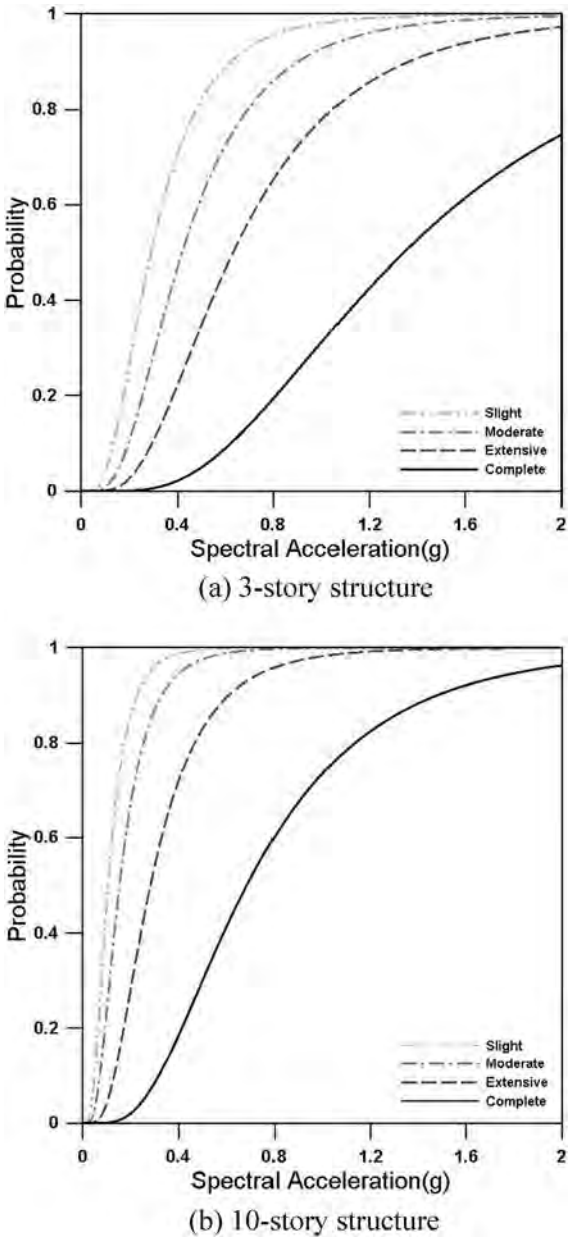

Fig. 12. Fragility curves of SMRF model structures.

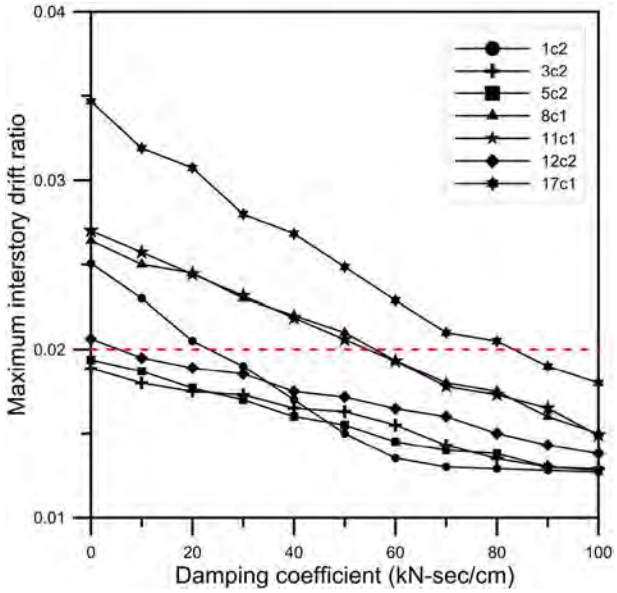

Fig. 13. Maximum inter-story drift ratios of the 3-story model structure with varying damping force of viscous dampers subjected to the seven earthquake records.

inter-story drift. Even though such devices have been proven to be effective in enhancing safety of structures, they have inherent disadvantage in that they tend to interrupt spatial planning or obstruct outside view. Recently, attempts have been made to install energy dissipation devices where the devices do not interfere with architectural planning ([7] for example. In this regard the special segment is a proper place for location of a damping device. As the special segment is subjected to large deformation only after plastic hinges form at both ends, the damper located in the special segment may not be effective for wind or low seismic loads.

In this section the effect of viscous dampers installed in the special segments was investigated. Fluid viscous dampers are known to reduce both stress and deflection within a structure simultaneously [25]. The dampers were designed in such a way that the displacement response of a STMF subjected to a certain earthquake, which is larger than the design earthquake, was reduced to a desired level. The damping force of a viscous damper, *F*, is generally expressed as follows.

$$F = c_d v^{\alpha} \tag{4}$$

where v is the relative velocity across the damper, c_d is the damping coefficient, and α is a constant exponent which is usually a value between 0.3 and 1.0. In this study α was assumed to be 1.0, which implies that the viscous damping force is linearly proportional to the velocity imposed on the damper.

In this study the objective of seismic retrofit of a STMF structure using viscous dampers placed in the special segments was set to enhance the seismic load resisting capacity of the model structure, which was originally designed for a seismic load with S_{DS} and S_{D1} equal to 0.43 and 0.23, respectively, in such a way that the structure satisfies the LS (life safety) performance level (maximum inter-story drift of 2% of story height) for an enhanced earthquake load with the design spectral response acceleration parameters $S_{DS} = 1.07$ and $S_{D1} = 0.79$, which corresponds to the design seismic load of Los Angeles area. Fig. 13 shows the maximum inter-story drift ratios of the 3-story model structure with a viscous damper in the special segments of all stories subjected to the seven earthquake records presented in Table 6, which are selected from the PEER NGA database. The records were scaled in such a way that the acceleration responses of the two model structures became equal to those of the enhanced design spectrum at the fundamental periods. The damping coefficient of the viscous damper was varied from 0 to 100 kN-sec/cm. It can be observed that as the damping coefficient increases the maximum inter-story drift gradually decreases. Through this parametric study, the viscous damping required to satisfy a target performance point can be determined. However such an approach may not be practical because a lot of computation is required to obtain a desired result.

Table 6
Seven earthquake records selected from the PEER-NGA database scaled to the enhanced seismic load.

PEER-NGA record information			PGA of scaled records	
Record seq. no.	Record ID.	File names (horizontal records)	3-story	10-story
953	1C1	NORTHR/MUL279, component 2	1.01 g	1.40 g
1602	3C2	DUZCE/BOL090, component 2	0.54 g	1.53 g
169	5C2	IMPVALL/H-DLT352, component 2	0.45 g	0.89 g
1116	8C1	KOBE/SHI000, component 1	0.53 g	0.83 g
900	11C1	LANDERS/YER270, component 1	0.50 g	0.49 g
848	12C2	LANDERS/CLW-TR, component 2	0.35 g	1.02 g
725	17C1	SUPERST/B-POE270, component 1	0.98 g	0.75 g

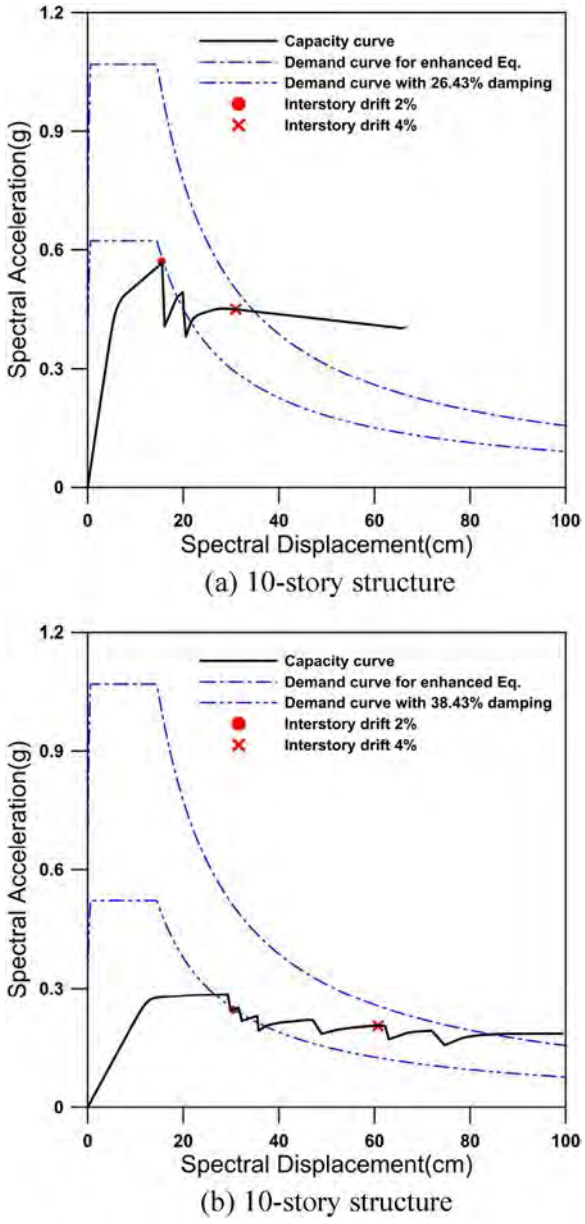

Fig. 14. Determination of the effective damping ratio required to satisfy the Life Safety performance point.

The required amount of additional viscous damping to meet a given performance objective for the enhanced earthquake load can be determined directly based on the nonlinear static procedure provided in the ASCE/SEI 41-10. In this approach the seismic performance point of a structure is obtained by plotting the demand and capacity curves on the same diagram, which is called a capacity-demand diagram. To this end the pushover curve is transformed into a capacity spectrum expressed in the spectral acceleration and displacement coordinates using the dynamic characteristics of the fundamental mode of vibration as follows:

$$S_a = \frac{V}{M_1^*} \quad S_d = \frac{\Delta_R}{\Gamma_1 \varphi_{R1}} \tag{5a, b}$$

where the modal participation factor, Γ_1, and the effective modal mass, M_1^*, for the fundamental mode are obtained as follows:

$$\Gamma_1 = \frac{\sum_{j=1}^{N} m_j \varphi_{j1}}{\sum_{j=1}^{N} m_j \varphi_{j1}^2} \quad M_1^* = \frac{\left(\sum_{j=1}^{N} m_j \varphi_{j1}\right)}{\sum_{j=1}^{N} m_j \varphi_{j1}^2}. \tag{6a, b}$$

The design spectrum is also plotted on the same diagram using the following relationship between the spectral displacement and acceleration:

$$Sd = \left(\frac{T^2}{4\pi^2}\right) S_a \tag{7}$$

The cross point of the two curves is regarded as the performance point. Fig. 14 shows the capacity curves of the 3 and 10-story STMF model structures and the 5% inherent damping demand curves for the enhanced earthquake load with the intensity of $S_{DS} = 1.07$ and $S_{D1} = 0.79$. It can be observed that significant displacement response occurred due to the enhanced earthquake. The maximum inter-story drift at the performance point turned out to exceed 4% of the story height. Also shown is the demand curve with 26.43 and 38.43% viscous damping which were found to satisfy the life safety limit states (maximum inter-story drift ratio of 2%) of the 3- and 10-story model structures. The demand curves with 26.43% and 38.43% damping ratio were drawn by dividing the 5% demand curve with the damping modification factors of 1.72 and 2.05, respectively, which were obtained using the following equation provided in the ASCE/SEI 41-10 Section 1.6.1.5.1.

$$B_1 = 4/[5.6 - \ln(100\beta_{eff})] \tag{8}$$

where B_1 is damping modification factor and β_{eff} is the effective viscous damping ratio.

When a linear viscous damper with damping constant C_j and inclination angle θ_j is installed in the vierendeel panel of the j^{th} story of a structure, the effective damping contributed from the added dampers can be estimated using the following formula provided in the ASCE/SEI 41-06:

$$\beta_{eff} = \beta + \frac{\sum_j W_j}{4\pi W_k} = \beta + \frac{\sum_j \left(\frac{2\pi^2}{T_{ss}} C_j \delta_{rj}{}^2\right)}{4\pi \left(\frac{1}{2}\sum_i F_i \delta_i\right)} = \beta + \frac{\sum_j \left(\frac{2\pi^2}{T_{ss}} C_j f_j{}^2 \varphi_{rj}{}^2\right)}{4\pi \left(\frac{2\pi^2}{T^2}\sum_i \left(\frac{w_i}{g}\right) \varphi_{im}{}^2\right)} \tag{9}$$

where β is the inherent damping ratio of 0.05, C_j is the damping coefficient of all dampers, f_j is $\cos\theta_j$, φ_{rj} is $\varphi_{jm} - \varphi_{(j-1)m}$, which is the difference between the displacements at the upper and lower ends of the dampers at the m^{th} mode vibration, w_i is the seismic weight, φ_{im} is the modal displacement at i^{th} level, T is the fundamental period of the rehabilitated building, and T_{ss} is the secant fundamental period of the rehabilitated building including the stiffness of the velocity dependent devices:

$$T_{ss} = T_i \sqrt{\frac{K_i}{K_s}} \tag{10}$$

where T_i is the elastic fundamental period (in seconds) in the direction under consideration calculated by elastic dynamic analysis, K_i is the elastic lateral stiffness of the building in the direction under consideration, and K_s is the secant stiffness at the target displacement.

To obtain the effective damping contributed from installation of dampers using Eq. (9), the relative displacement between two ends of the dampers at a vibration mode needs to be computed. Fig. 15 shows the deformed configuration of a single span STMF with a viscous damper in the special segment, and the relationship between the lateral displacement and the damper deformation was obtained as follows based on the assumption that the lateral displacement is relatively small compared with the story height and there is no change in the length of the chords in the vierendeel panels. The inter-story drift, δ, of a story can be obtained as.

$$H \cdot \theta = \delta \tag{11}$$

where H is the story height and θ is the rotation of the story. From the geometry of the deformed special segment, the length of the diagonal after deformation can be obtained as follows

$$l_{vd}' = \sqrt{[H_s]^2 + [B_s + (H_s \tan\theta_s)]^2} \tag{12}$$

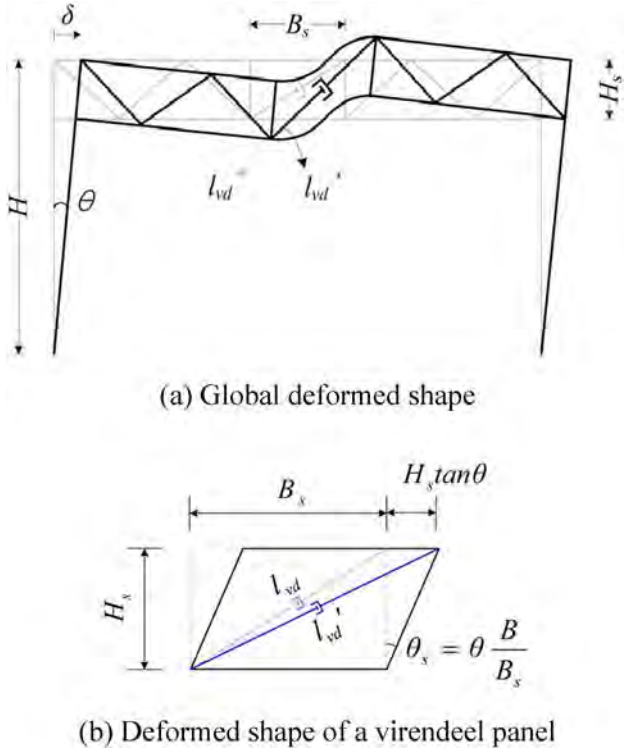

Fig. 15. Deformed configuration of a STMF structure with a viscous damper in the special segments.

where H_s and B_s are the height and width of the special panel, and θ_s is the rotation of the special panel. The rotation of the special panel is proportional to the rotation of the column and span length, and is inversely proportional to the length of the special segment, B_s, as follows.

$$\theta_s = (\theta \cdot B)/B_s \tag{13}$$

Using Eq. (13) the length of the diagonal after deformation, Eq. (12), can be modified as follow

$$l_{vd}' = \sqrt{[H_s]^2 + \left[B_s + \left\{H_s \tan\left(\frac{\delta B}{B_s H}\right)\right\}\right]^2}. \tag{14}$$

The above approach was applied to the model structures to determine the required damping coefficient to satisfy the *LS* (life safety) performance point for the enhanced earthquake load. Based on the characteristics of the plastic hinge formation depicted in Fig. 7, viscous dampers were placed in the 1st and the 2nd stories in the 3-story structure and in the 2nd to 9th stories in the 10-story structure, damping constants of 65.44 kN-sec/cm and 42.24 kN-sec/cm were obtained for the 3- and the 10-story structures, respectively, using Eq. (9).

Fig. 16 depicts the maximum inter-story drift ratios of the model structures before and after retrofit with viscous dampers subjected to seven ground motions with enhanced intensity selected from the 44 ground motions used in the fragility analysis. The characteristics of the earthquakes used in the analysis are presented in Table 6. The earthquake records were scaled in such a way that the spectral acceleration at the fundamental period of each model structure was equal to the corresponding value of the design spectrum enhanced to the desired intensity. It can be observed that the maximum inter-story drifts of the original structures exceed the limit states of 2% of story height when subjected to the enhanced seismic loads, whereas those of the

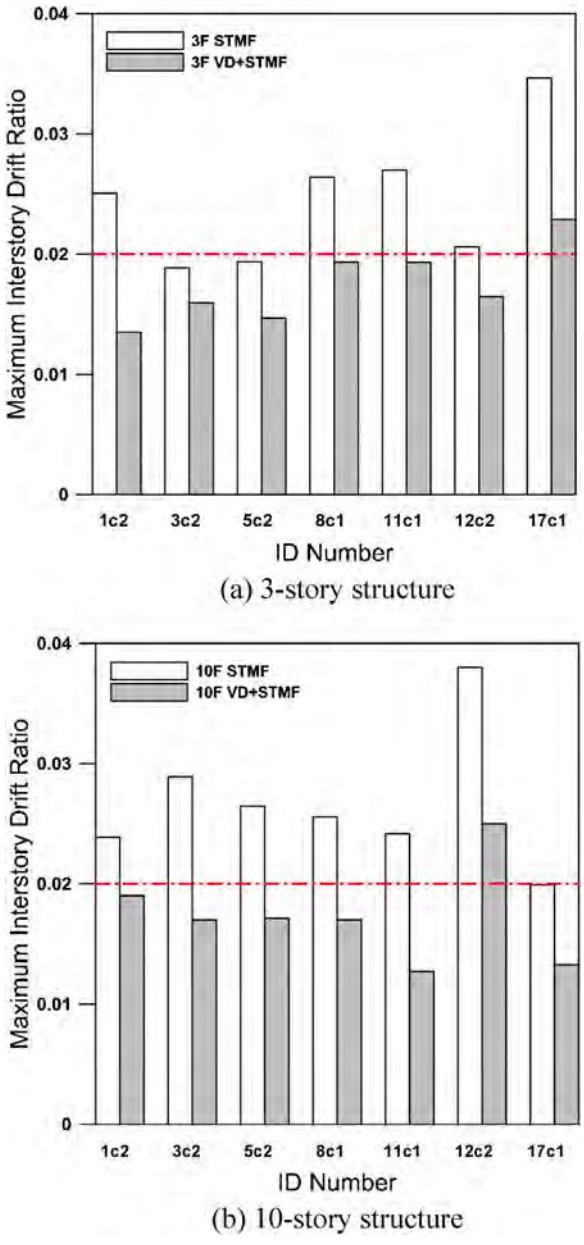

Fig. 16. Maximum inter-story drift ratios of the model structures before and after retrofit with viscous dampers subjected to the seven ground motions.

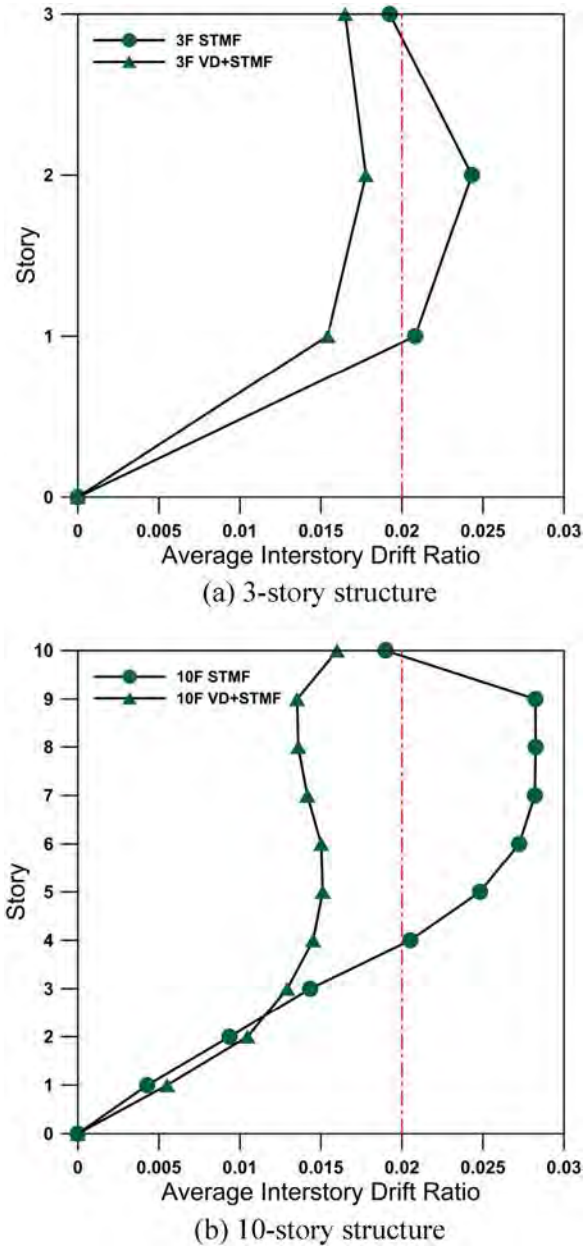

Fig. 17. Mean maximum inter-story drift ratios of the STMF model structures before and after retrofit with viscous dampers subjected to the enhanced earthquakes.

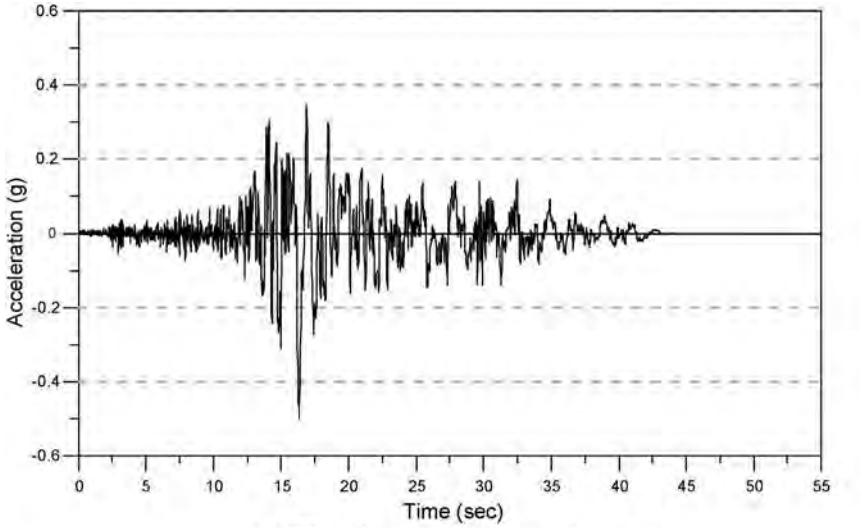

(a) Time history of the earthquake

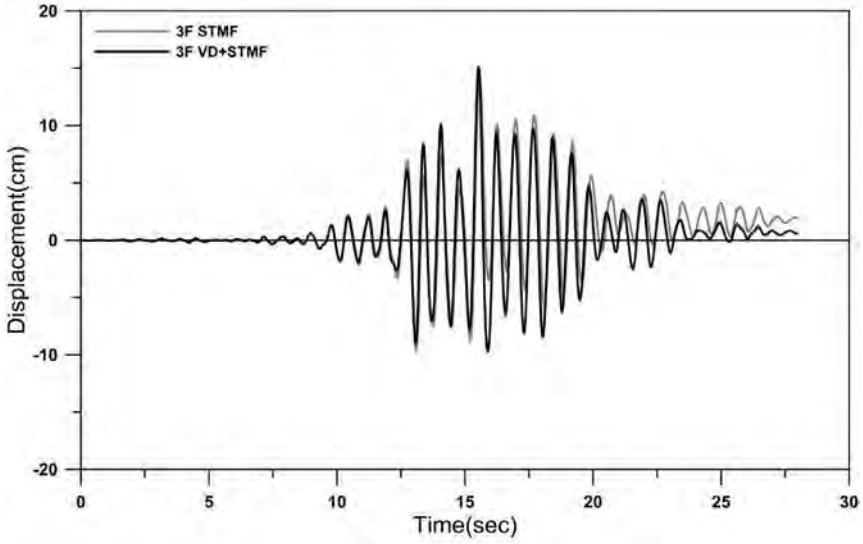

(b) 3-story structure

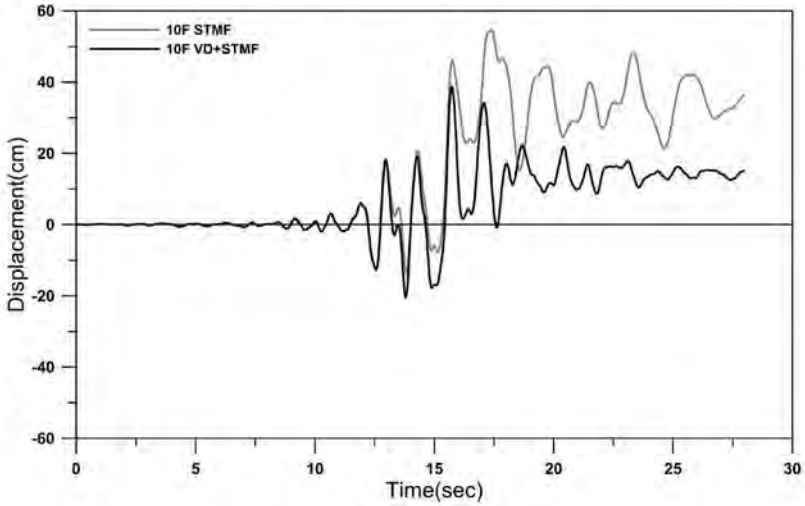

(c) 10-story structure

Fig. 18. Roof displacement time histories of the model structures subjected to Landers earthquake.

structures reinforced with viscous dampers are smaller than the limit states for most earthquake records used in the analysis. In the case of the 3-story structure with viscous dampers, only the inter-story drift for the Superstition Hills earthquake exceeded the given limit state. In the 10-story structure the maximum inter-story drift of the retrofitted structure exceeded the desired limit state when subjected to the enhanced Northridge earthquake due to large inter-story drift at the 10th story where no damper was installed.

Fig. 17 shows the mean maximum inter-story drift ratios of the model structures before and after retrofit with viscous dampers subjected to the seven earthquakes with enhanced intensity. The vertical alternated long and short dash line represents the target inter-story drift ratio of 2%. It can be observed that the mean maximum inter-story drifts in all stories are reduced below the target value after the dampers are installed. In the 3-story structure the inter-story drift of the first and the second stories were reduced by 26%, and that of the third story, where no damper was installed, was reduced by 14%. In the 10-story structure the inter-story drifts of the first and the second stories, where dampers were not installed, rather increased. However in the other stories the reduction in the mean inter-story drift is as large as 36%.

Fig. 18 shows the time histories of the roof story displacement of the model structures due to Landers earthquake scaled to meet the enhanced design spectrum. It can be observed that after the dampers were installed the reduction in the maximum displacement at the roof story is only marginal, while the decrease in the residual displacement is rather significant.

Fig. 19 shows the plastic hinge formation in the 3-story structures with and without viscous dampers subjected to the Landers earthquake. In both structures plastic hinges occurred at the first and the second story special segments. It can be observed that in the original structure the plastic rotations in the plastic hinges ranged from 50 to 90% of the CP (collapse prevention) state. In the structure with viscous dampers in the special segments the number of plastic hinges was reduced to 3/4 of the original structure and the amount of plastic rotation was reduced to 50% of the CP state in every plastic hinge.

Table 7
Median structural capacity, $\hat{C}$ of the model structures with viscous dampers obtained from incremental dynamic analyses.

	Slight	Moderate	Extensive	Complete
3-story with VD	0.33	0.49	0.78	1.7
10-story with VD	0.11	0.17	0.29	1.0

The incremental dynamic analysis results of the structures with viscous dampers obtained using the 44 earthquake records used previously are shown in Fig. 19. From the analysis results the median capacity of the structure corresponding to each damage state was obtained and is presented in Table 7. It can be observed that the median capacities of the STMF structures with viscous dampers are slightly higher than those of the structures without dampers presented in Table 5. It also can be noticed that the difference in median capacity increases as the damage state becomes more severe.

Fig. 20 depicts the incremental dynamic analysis results of the structures with viscous dampers obtained using the 44 earthquake records. Fig. 21 shows the fragility curves of the structures with viscous dampers obtained using the incremental dynamic analysis results and Eq. 3. The fragility curves of the model structures without dampers shown in Fig. 11 are also plotted for comparison. It can be observed that the probability of reaching a limit state for a given seismic intensity decreased only slightly in the slight and the moderate damage states. However the decrease in the failure probability is most significant in the complete damage state. This is due to the fact that for earthquakes

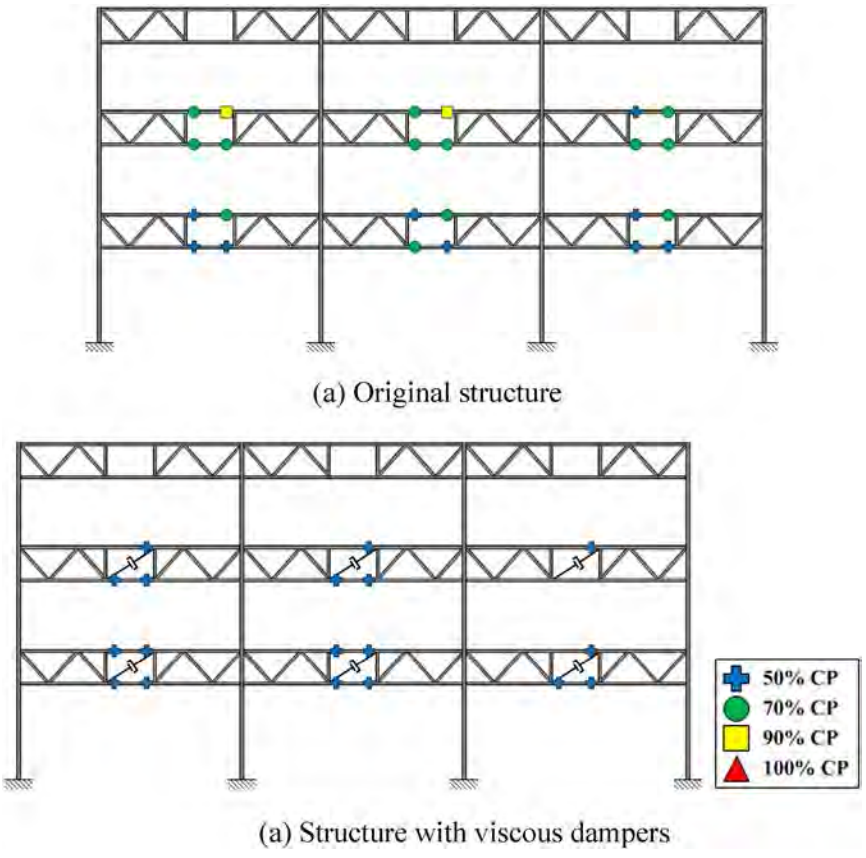

Fig. 19. Plastic hinge formation in the 3-story structures subjected to the Landers earthquake.

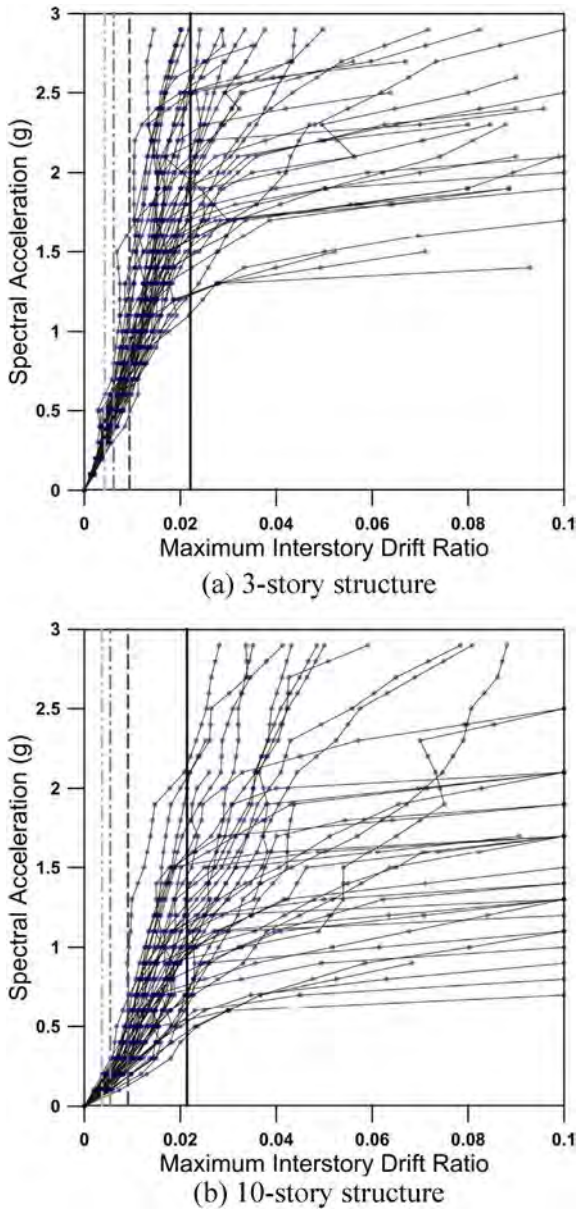

Fig. 20. Incremental dynamic analysis results of the structures with viscous dampers.

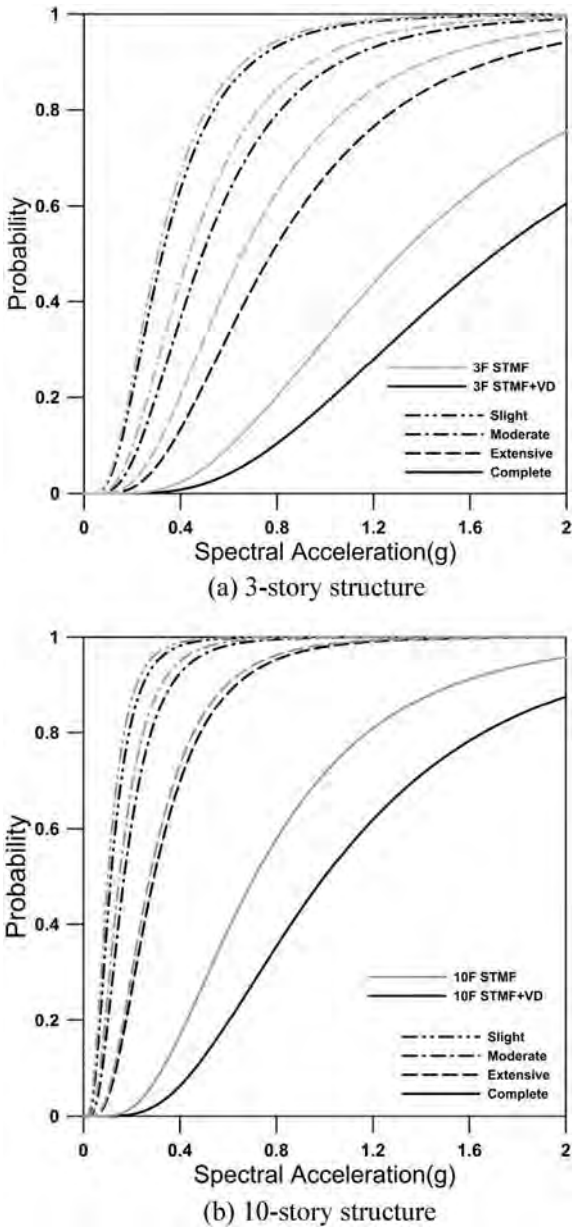

Fig. 21. Comparison of fragility curves of the model structures with and without viscous dampers.

with small to moderate intensity the relative displacement between the upper and the lower chords is quite small, which results in marginal effectiveness of the viscous dampers. However for complete damage state which is associated with large deformation, the contribution of the dampers become more significant.

5. Conclusions

In this study the seismic performance of STMF was investigated by fragility analyses and the results were compared with the performance of special moment resisting frames. Then seismic retrofit scheme was proposed by installing a viscous damper in the special segment.

Pushover analysis results showed that STMF model structures generally have larger stiffness and strength than those of the SMRF structures designed with the same loading condition. However ductility was slightly reduced in comparison with the moment frames. It was also observed that, as assumed in the design phase, most plastic hinges formed at the chord members in the special segments, and that failure occurred when the plastic rotation in the special segments exceeded the limit state. Nonlinear dynamic analysis showed that the seismic retrofit of STMF structures using viscous dampers in the special segments resulted in reduction of the maximum inter-story drifts below the desired target point. The capacity-demand diagram method provided in the ASCE/SEI 41-10 turned out to be effective in estimating the required amount of additional viscous damping to meet a given target performance point. According to fragility analysis results, the probabilities of reaching a limit state of STMF were similar to those of the SMRF structures. The probability of reaching a limit state for a given earthquake intensity was higher in the 10 story structure than that of the 3 story structure. It was also observed that the seismic performance of STMF was marginally increased by installation of viscous dampers in the special segments in the slight to moderate damage states. The effect of the viscous dampers on enhancing seismic safety of STMF increased significantly in the complete damage state which is associated with large deformation in the special segments.

Acknowledgement

This research was supported by a grant (13AUDP-B066083-01) from Architecture & Urban Development Research Program funded by Ministry of Land, Infrastructure and Transport of Korean government.

References

[1] AISC, Seismic Provisions for Structural Steel Building, AISC-341-10, American Institute of Steel Construction, Chicago, Illinois, 2010.
[2] AISC, Specification for Structural Steel Buildings, American Institute of Steel Construction AISC, Chicago (IL), 2007.
[3] ASCE, Minimum Design Loads for Buildings and Other Structures (ASCE/SEI 7-13), American Society of Civil Engineers, Reston, 2013 2013.
[4] ASCE/SEI 41-10, Seismic Evaluation and Retrofit of Existing Buildings, American Society of Civil Engineers, Reston, 2010.
[5] H. Basha, S.C. Goel, Seismic Resistant Truss Moment Frames with Ductile Vierendeel Segment, Report No. UMCEE 94-29, Dept. of Civ. & Env. Engrg., Univ. of Michigan, Ann Arbor, Michigan, 1994.
[6] S.H. Chao, S.C. Goel, Performance-based plastic design of special truss moment frames, Engineering Journal (2008) 127–150.
[7] K.S. Choi, H.J. Kim, Strength demand of hysteretic energy dissipating devices alternative to coupling beams in high-rise buildings, International Journal of High-Rise Buildings 3 (2) (2014) 107–120.
[8] C.A. Cornell, F. Jalayer, R. Hamburger, D. Foutch, Probabilistic Basis for 2000 SAC Federal Emergency Management Agency Steel Moment Frame Guidelines, Journal of Structural Engineering (2002).
[9] FEMA P695, Quantification of Building Seismic Performance Factors, Federal Emergency Management Agency, 2009.
[10] S.C. Goel, A.M. Itani, Seismic behavior of open-web truss-moment frames, J. Struct. Eng. 120 (6) (1994).
[11] A.A. Farghaly, Seismic analysis of 3-D two adjacent buildings connected by viscous dampers with effect of underneath different soil kinds, Smart Structures and Systems 15 (5) (2015) 1293–1309.
[12] A. Heidari, S. Gharehbaghi, Seismic performance improvement of special truss moment frames using damage and energy concepts, Earthq. Eng. Struct. Dyn. 44 (7) (2015) 1055–1073.
[13] S.J. Jordan, S. Elfass, G. Pekcan, Seismic Response Investigation of Special Truss Moment Frame Subassemblies under Quasi-Static Loading, Proceedings of the 2007 Earthquake Engineering Symposium for Young Researchers, Seattle, Washington, 2007.
[14] J. Kim, S. Lee, H. Choi, Progressive collapse resisting capacity of moment frames with viscous dampers, Struct. Des. Tall Special Build. 22 (5) (2013) 399–414.
[15] J. Kim, J. Park, Design of Special Truss Moment Frames Considering Progressive Collapse, International Journal of Steel Structures 14 (2) (2014) 1–13.
[16] O. Lavan, R. Levy, Performance based optimal seismic retrofitting of yielding plane frames using added viscous damping, Earthquakes and Structures 1 (3) (2010).
[17] H.D. Ölmez, C. Topkaya, A numerical study on special truss moment frames with vierendeel openings, J. Constr. Steel Res. 67 (4) (2011) 667–677.
[18] G. Pekcan, A. Itani, C. Linke, Damage avoidance design of special truss moment frames with energy dissipating devices, J. Constr. Steel Res. 65 (6) (2009) 1374–1384.
[19] G. Pekcan, C. Linke, A. Itani, Enhancing seismic resilience using truss girder frame systems with supplemental devices, J. Constr. Steel Res. 94 (2014) 23–32.
[20] PEER, PEER NGA Database, Pacific Earthquake Engineering Research Center, University of California, Berkeley, U.S.A., 2006http://peer.berkeley.edu/nga/.
[21] PERFORM-3D, Nonlinear analysis and Performance Assessment for 3D Structures-User Guide, Computers and Structures, Berkeley (CA, USA), 2006.
[22] D. Philippe, Considerations in the design of viscous dampers used to suppress wind-induced vibration in high-rise buildings, Proceedings of the 8th International Conference on Structural Dynamics, EURODYN 2011, Leuven, Belgium, 2011 4–6 July.
[23] M.H. Serror, A. Adel diab, M. SA, Seismic force reduction factor for steel moment resisting frames with supplemental viscous dampers, Earthquakes and Structures 7 (6) (2014) 1171–1186.
[24] S. Silvestri, G. Gasparini, T. Trombetti, Seismic design of a precast r.c. structure equipped with viscous dampers, Earthquakes and Structures 2 (3) (2011) 297–321.
[25] D.P. Taylor, P. Duflot, Fluid Viscous Dampers Used for Seismic Energy Dissipation in Structures, Taylor Devices Inc., Report, 2005.
[26] A.S. Tzimas, A.I. Dimopoulos, T.L. Karavasilis, EC8-based seismic design and assessment of self-centering post-tensioned steel frames with viscous dampers, J. Constr. Steel Res. 105 (2015) 60–73.